Remote Sensing for Active Volcano Monitoring in Barren Island, India*

Abstract

The Barren Island Volcano, situated in the Andaman Sea of the Bay of Bengal, erupted recently (March, 1991) after a prolonged period of quiescence of about 188 years. This resumed activity coincides with similar outbreaks in the Philippines and Japan, which are located in an identical tectonic environment. This study addresses (1) remote sensing temporal monitoring of the volcanic activity, (2) detecting hot lava and measuring its pixel-integrated and sub-pixel temperatures, and (3) the importance of SWIR bands for high temperature volcanic feature detection. Seven sets of TM data acquired continuously from 3 March 1991 to 8 July 1991 have been analyzed. It is concluded that detectable pre-eruption warming took place around 25 March 1991 and volcanic activity started on 1 April 1991. It is observed that high temperature features such as an erupting volcano can register emitted thermal radiance in SWIR bands. Calculation of pixel-integrated and sub-pixel temperatures related to volcanic vents has been made, using the dual-band method.

Figure 1. Location map of Barren Island.

Introduction

Volcanic eruptions are natural hazards that destroy human property and lives, and leave a long-lasting impact on the environment by virtue of spewing large quantities of carbon dioxide and sulphur dioxide into the atmosphere. It is worthy to study volcanic events through remote sensing techniques, as the event provides a remarkable opportunity to study the ongoing magmatism and the associated various volcanologic features, thereby giving chances to deduce the interior composition and structure of the Earth.

There exists only a limited opportunity for frequent physical observations, gas and rock sampling, temperature measurements, etc. at the Barren Island Volcano because the area is quite remote from the mainland. It is especially inaccessible during the time of eruption and the monsoon season. Thus, the present work has utilized remote sensing technology for studying the various features of the recent volcanism on Barren Island. Temporal data analysis of Barren Island volcanic activity is an excellent example of the surveillance capabilities of the satellite remote sensing technology.

Objectives

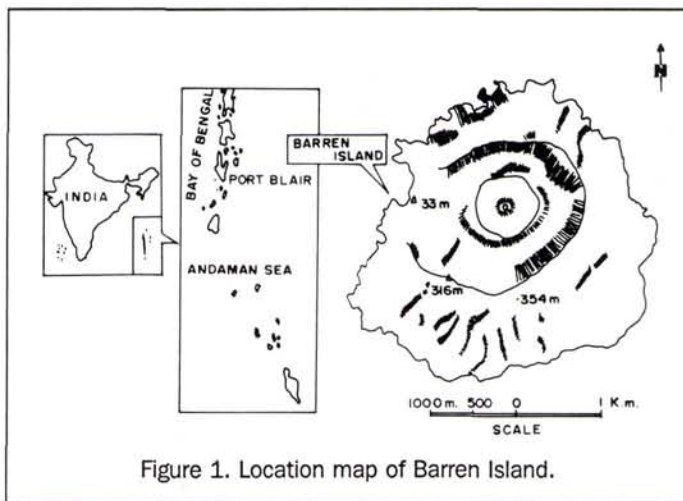The study addresses (1) remote sensing temporal monitoring of the volcanic activity; (2) location and mapping of new volcanogenic products, such as lava, pyroclastic, and debris flows; (3) detection of hot lava and measurement of its pixel-integrated and sub-pixel temperatures; and (4) the importance of SWIR bands for high temperature volcanic feature detection.

Location of the Study Area

The Barren Island Volcano, situated in the Andaman Sea of the Bay of Bengal, is the only known active volcano in India. The island is 130 km east-northeast of Port Blair town (Figure 1) and covers an area of about 8.3 sq km. The study area is covered by Survey of India topographic sheet no. 86 H/15 and lies between latitudes 12° 15' and 12° 20' N and longitudes 93° 48' and 93° 55' E.

Geology and Geomorphology of Barren Island

The Barren Island Volcano, composed mainly of andesitic rocks, formed about a million years ago due to submarine volcanic activity. The satellite images shown in Plate 1 provide synoptic and multi-temporal views of the Barren Island Volcano. The amphitheater-like landform with a dark-toned inner rim is easily discernible. This is the breached caldera with a diameter of about 3 km. Luxuriant vegetation on the outer slopes indicates deep weathering and soil formation. Within this, at the center of the island, occurs a small cinder cone built of lava erupted during the last episode. A small crater occurs on top of the cone. The cone rises from the sea floor to a height of 311 m above mean sea level and is nearly symmetrical in cross section with a circular base in plan

A. Bhattacharya
C. S. S. Reddy
S. K. Srivastav
National Remote Sensing Agency,
Hyderabad, Andhra Pradesh, India.

TM MULTI-TEMPORAL DATA ANALYSIS
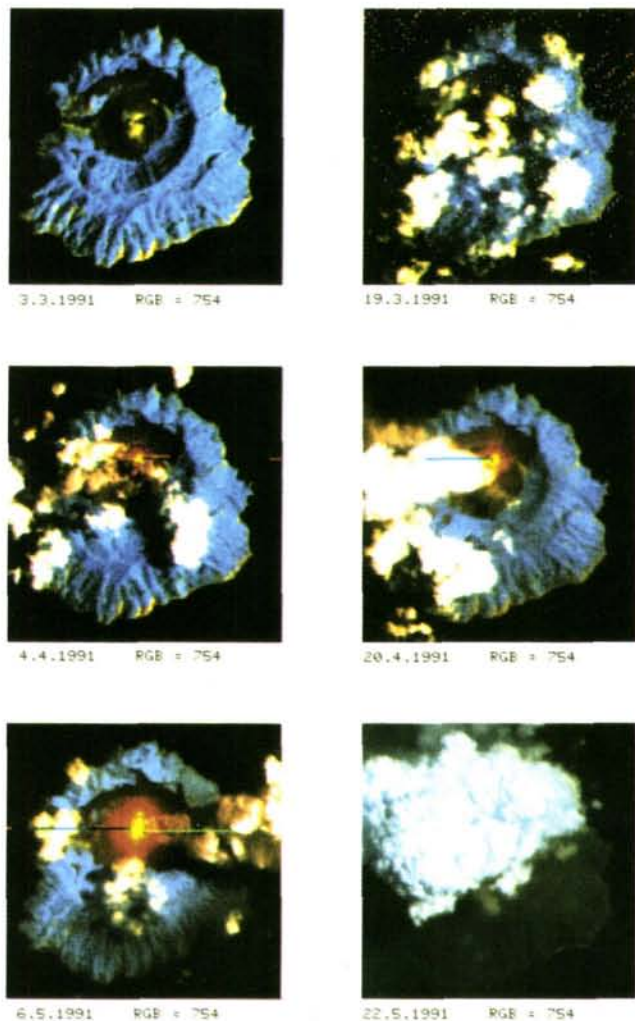## OF BARREN ISLAND VOLCANO

Plate 1. Co-registered multitemporal TM imagery of Barren Island. Refer above images as (a) 3 Mar 91, (b) 19 Mar 91, (c) 4 Apr 91, (d) 24 Apr 91, (3) 6 May 91, and (f) 22 May 91.
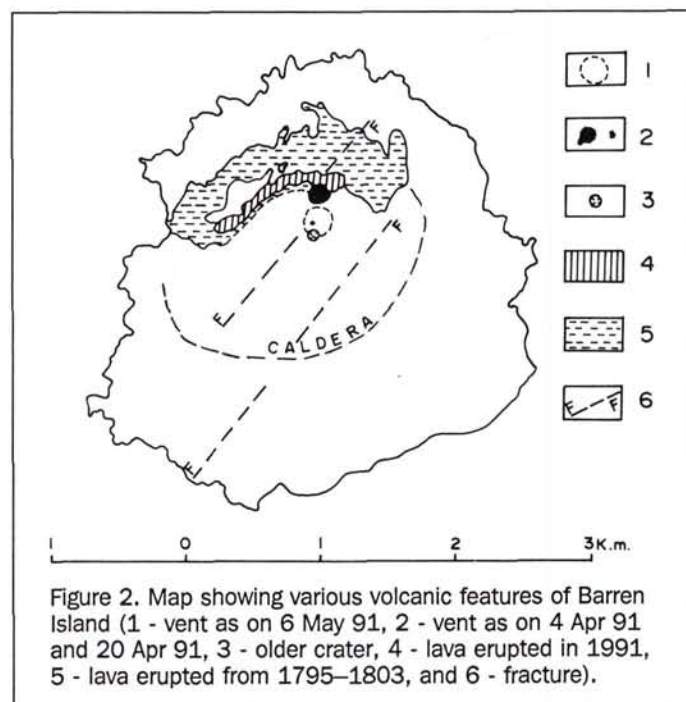
Recent Eruption and Resulting Features

Based on the visual interpretation of digitally enhanced raw data, mainly False Color Composite (FCC) of bands 754, 654, and 745, a generalized map of the area (Figure 2) has been prepared showing various volcanic features. The older flows and centrally located cinder cone that have formed during the 1795 to 1803 eruption have been delineated by virtue of their tonal differences from the surrounding rocks. They have typical dark tones and are devoid of vegetation due to the lack of development of thick soil which could support plant growth.

However, recent lava flows have bright (light) tones on thermal IR data because of their hot nature. The map also shows the varying position and size of the vents that were activated during the present episode. Two prominent parallel fractures trending northeast-southwest, one of which passes directly through the vent, have also been demarcated on this map. Further, it could be inferred that these fractures are of recent origin because they cut across lava flows that have erupted during the last volcanic episode 188 years ago.

As far as the lava flow is concerned, TM FCC (654 = RGB) shown in Plate 2 (acquired on 6 May 1991) clearly depicts the westward flow of the lava towards the Bay of Bengal. The lava did not reach the coast until 6 May 1991 and is about 200 m inland from the sea shore. The image acquired on 22 May 1991 (Plate 1f) though portrays a giant umbrella cloud over the caldera, but actually it is dense smoke which has been established through its digital numbers and the absence of cloud in the surrounding sea. The cauliflower-like shape of the smoke plume along with the dense ash cover seen throughout the island (due to which the vegetation has very low reflectance in band 4) leads to the conclusion that the eruption was of vulcanian type and was intensified during the course of time.

Remote Sensing of Barren Island

The Barren Island Volcano is covered in quadrant no. 1 of path 133 and row 52 of Landsat 5 satellite and LISS-II A1

view. Materials thrown in gas-generated explosions accumulate around the vent to form a steep sided cone.

In Plate 1a, the central cone and the surrounding lava flows are clearly visible in dark tones and are conspicuous due to the absence of vegetation. These are the volcanic products that were formed during the last eruption (1795 to 1803) as reported in the memoirs of the Geological Survey of India (GSI). In 1795, the volcano erupted cinders and blocks weighing a few tonnes. Enormous clouds of gases and vapors were also generated. Sulphurous emanations on the wall of the volcano led scientists to think that Barren Island had gone into a solfatoric (waning) stage (Radhakrishnan, 1987). However, the recent eruption was quite unexpected and took many geologists by surprise.

Figure 2. Map showing various volcanic features of Barren Island (1 - vent as on 6 May 91, 2 - vent as on 4 Apr 91 and 20 Apr 91, 3 - older crater, 4 - lava erupted in 1991, 5 - lava erupted from 1795–1803, and 6 - fracture).
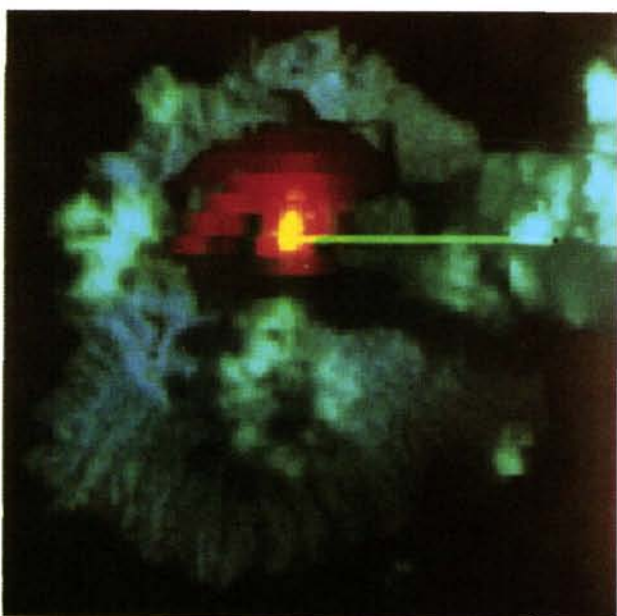
Plate 2. Image acquired on 6 May 1991 showing westward movement of lava flow.
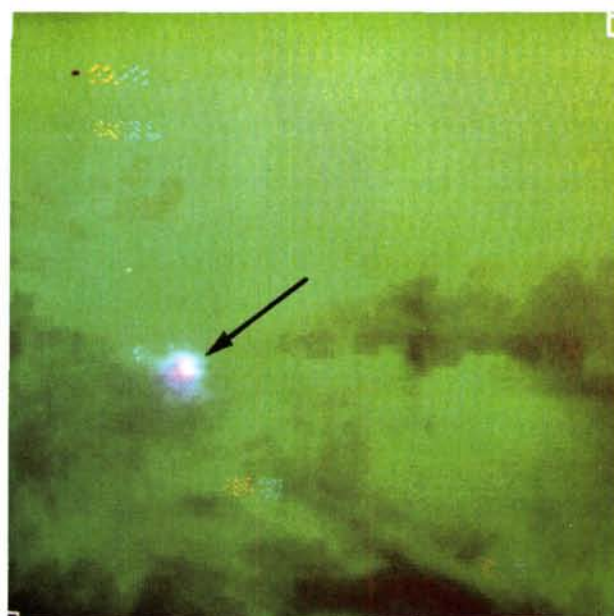

Plate 3. Nighttime FCC 567 = BGR acquired on 8 July 1991. Arrow indicates thermally radiant pixels.
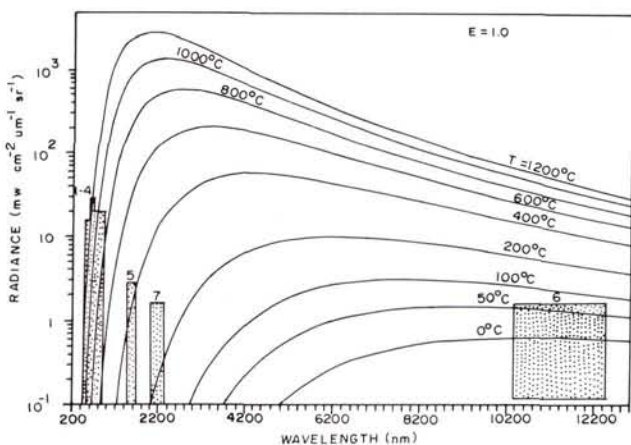

Figure 3. Wavelength dependence of thermal radiance of black body.

scene of IRS-1A path 11 and row 60. Seven sets of TM data acquired continuously from 3 March 1991 to 8 July 1991 have been analyzed. In addition to these data sets, several TM scenes for the period June through October 1991, were browsed but were found to be cloud covered. Smoke plumes could be detected on the IRS-1A FCC. Thematic Mapper data of 6 May 1991 showed only one anomalous pixel which was thermally radiant enough to be registered in band 4. In addition, the TM night time pass (5 −193) acquired on 8 July 1991, consisting of all seven bands, has also been analyzed.

SWIR Data for Volcanic Studies
Francis and Rothery (1987) and Rothery et al. (1988) have recently drawn attention to the potential use of Short Wave-

length Infrared (SWIR) satellite data for the detection and monitoring of the thermal events at volcano sites. The SWIR region of the electromagnetic spectrum ranges from 1.0 to 3.0 μm, which is also known as the reflected infrared region. This region is commonly regarded as suitable for studying the reflectance properties of vegetation, soils, and rocks. Earth surface features, at normally prevailing temperatures, emit very small quantities of radiation in this region and radiate mostly in the thermal infrared region, where there is negligible reflected solar radiation. However, certain terrian features, such as an erupting volcano, have high temperatures on the order of 1000 °C and emit radiation in SWIR region as dictated by Planck's formula.

Figure 3 shows the thermal radiance at temperatures ranging from 0 °C to 1200 °C as a function of wavelength for a uniform emissivity of 1.0. The boxes represent the band-passes and operational range of radiance covered by the visible, SWIR, and thermal IR channels of the Landsat Thematic Mapper sensor. It is evident from Figure 3 that TM bands 7 and 5 can be used to measure temperatures from 160 °C to 220 °C and 250 °C to 420 °C, respectively, assuming that all the at-satellite radiance is of thermal origin. Similarly, TM bands 1 to 4 are capable of measuring pixel-integrated temperatures from 700 to 1200 °C. Between the saturating levels of band 5 and lower sensitivity limit of band 4, there is a gap in the coverage of pixel-integrated temperatures from 420 to 700 °C. But we all know that thermal radiance at shorter wavelengths is combined with solar radiance which is reflected by the surface. Therefore, in order to calculate the temperatures from emitted SWIR, one has to account for the reflected component. This was achieved as follows:

It is regarded that the volcanic rock surrounding the crater has the same reflectance in both the pre-eruption 3 March 1991 and during eruption 4 April 1991 to 6 May 1991 images. Then the reflected component can be roughly estimated form the pre-eruption 3 March 1991 image. Thus, emitted ra-

diance of the thermally radiant target has been obtained by subtracting the reflected component from the total detected radiance during the eruption. For this purpose, the effective near-nadir reflectance form both the surface and the atmosphere has been calculated following the formula given by Markham and Barker (1986).

Image Registration

Raw TM data (geometrically uncorrected) sets formed the basic dataset for further analysis. Image to image registrations have been carried out taking 3 March 1991 data as the master image, to which later dates were adjusted. This helped us to calculate the reflected radiance of the volcanic rocks surrounding the vent using the pre-eruption and post-eruption (for non-thermally radiant pixels of fresh lava) data. Co-registration of images has also facilitated multi-temporal analysis. Maximum care has been taken to ensure proper registration, and the RMS error is as low as 0.22 in the pixel direction and 0.32 in the along line direction. For the purpose of resampling, the nearest neighbor algorithm has been used, which does not alter original pixel values considerably in a small image containing 128 pixels by 128 lines. Plate 1 shows the data sets after image to image geometric corrections have been made.

Calculation of Pixel-Integrated Temperatures.

An ASCII printout of digital numbers has been taken for a small subset window of 20 pixels by 18 lines covering the vent area in all the data sets. The first step in temperature calibration of the grey values is to convert the raw digital numbers into spectral radiance. From the emitted radiance, pixel-integrated temperatures have been calculated by using Planck's formula. An emissivity value of 0.8 was used for the temperature calculations using TM bands 4, 5, and 7.

The pixel-integrated temperatures should be regarded as a minimum estimate of radiant temperature of the hottest material in the pixel (Rothery et al., 1988; Pieri et al., 1990). Thus, a small portion of the pixel which is radiating at high temperature is averaged over the entire pixel area. This sub-pixel temperature can be determined by the following method.

Calculation of Sub-Pixel Temperatures

Apparent (pixel-integrated) temperatures and DN which would be measured by the Landsat TM for a variety of volcanic features are given by Rothery et al. (1988). The same pixel-integrated temperatures were not found for any given pixel in two spectral bands. This is due to the wavelength-dependent relationship between radiance and temperature, so that pixels which contain sub-pixel size radiant areas appear hotter at shorter wavelengths. If we assume that the highly radiant proportion of the pixel is the same in each of two spectral bands such as TM 5 and 7, then we can use this relationship to determine the highly radiant proportion of a pixel for which the derived temperatures are the same in each band. This technique, known as the dual-band method, was developed by Matson and Dozier (1981) and modified and adopted for volcanic studies by Rothery et al. (1988). The dual-band method provides a means of estimating both size and temperature of hot areas which occupy less than a complete pixel.

Results and Discussions

Thematic Mapper data obtained on 3 March 1991 do not show any significant temperature anomalies related to the volcanic eruption. Thermal IR data (Band 6) have shown certain warm signatures. However, close examination of the data revealed that they are due to strong solar illumination. Thus, it seems that detectable pre-eruption warming had not taken place by 3 March 1991. The data obtained on 19 March 1991 did not show any definite signs of eruption. However, these data are of poor quality and partially cloud covered which could be responsible for the lack of any detectable signatures.

Clearcut indications of the volcanic eruption can be seen from 4 April 1991 onwards until 8 July 1991 (later dates of Landsat and IRS passes until 30 October 1991 were cloud covererd). Thus, the eruption took place sometime between 19 March and 4 April 1991. In order to further narrow down the exact commencement date of the volcanic eruption, AVHRR images acquired on a daily basis have been checked back through 4 April 1991. This examination led to the identification of possible beginning of the event on 1 April 1991 and the pre-eruption warming beginning sometime around 25 March 1991.

The TM data obtained on 4 and 20 April 1991 show around 16 pixels saturated in Band 7. However, only six pixels are saturated in band 5, indicating that the pixel-integrated temperatures are more than 420 °C in the central part of the vent. There are no detectable thermally radiant pixels in band 4, which suggests that the pixel-integrated temperatures are less than 700 °C. Because the saturated pixels cannot be used for finding the sub-pixel temperatures, unsaturated pixels in band 5 and 7 adjacent to the core region have been taken to calculate the size and sub-pixel temperatures of the hot molten lava. For this purpose, the background temperature of 200 °C has been assumed (Rothery et al., 1988; Piere et al., 1990) and the sub-pixel temperatures have been calculated. The sub-pixel temperatures range between 787 to 807 °C for 4 April 1991 and 20 April 1991 and the hot proportion of the pixel varies between 0.0022 and 0.0026 corresponding to 1.98 and 2.34 sq m, respectively.

The 4 April 1991 image clearly shows a thermal anomaly in bands 5, 6, and 7 which is located about six pixels towards the south of the main vent, which was activated initially. This is interpreted as a magmatic precursor to the latest volcanic eruption and forms the prime contribution of this study. The above observation is clearly evident on the 6 May 1991 image wherein the size and the position of the vent have changed substantially. This clearly suggests the presence of at least two vents which were activated in this volcanic episode.

There are about 45 pixels saturated in band 7 and 18 in band 5 on the 6 May 1991 data. In addition, one pixel is thermally radiant enough to be registered in band 4, which indicates a pixel-integrated temperature of at least 700 °C and above. Thus, it seems that the volcanic activity was intensified during the course of time. Thick ash cover around the cone and on the surrounding forests (Plate 1f) further confirms the above observation. Dual band method indicates sub-pixel temperatures varying between 637 to 887 °C and occupying a sub-pixel area of about 6.0 sq m.

All seven bands of the nighttime Landsat TM data acquired on 8 July 1991 were analyzed and revealed thermally radiating pixels in bands 5, 6, and 7 (Plate 3). It can be considered clear evidence of the capability of short wavelength infrared (SWIR) bands (TM 5 and 7) in detecting and monitoring the high temperature geoenvironmental features, such as the volcanic eruption of Barren Island in the present case. In the absence of solar radiation at night, the signal recorded by the sensors operating in SWIR bands consists primarily of

thermal radiation emitted by the erupting volcano. Therefore, it is possible to calculate the pixel-integrated temperatures directly without due regard to the reflected radiation.

The nighttime TM band 5 data obtained on 8 July 1991, show about 120 thermally radiating pixels whereas band 7 data show about 160 thermally radiating pixels. Thus, the calculated pixel-integrated temperatures range from 265 to 392 °C in band 5 and 152 to 281 °C in band 7. The dual band method suggests a sub-pixel temperature for the vent as high as 1177 °C radiating at 0.00095 proportion of a pixel. The temperatures of the freshly erupting lava usually range between 500 and 1400 °C (Radhakrishnan, 1987), which corroborates well with the results obtained in this study.

Acknowledgments

References

Francis, P. W., and D. A. Rothery, 1987. Using the Landsat thematic mapper to detect and monitor active volcanoes: An example from Lascar volcano, northern Chile, *Geology*, 15:614–617.

Markham, B. L., and J. L. Barker, 1986. Landsat MSS and TM postcalibration dynamic ranges, exoatmospheric reflectances and at-satellite temperatures, *EOSAT Tech. Notes 1*, Earth Observation Satellite Company, Lanham, Maryland, pp. 3–8.

Matson, M., and J. Dozier, 1981. Identification of subresolution high temperature sources using a thermal IR sensor, *Photogrammatric Engineering & Remote Sensing*, 47:1311–1318.

Pieri, D. C., L. S. Glaze, and M. J. Abrams, 1990. Thermal radiance observations of an active lava flow during the June 1984 eruption of Mount Etna. *Geology*, 18:1018–1022.

Radhakrishnan, V., 1987. *General Geology*, V.V.P. publishers, Tuticorin, India, 406 p.

Rothery, D. A., P. W. Francis, and C. A. Wood, 1988. volcano monitoring using short wavelength infrared data from satellites. *Journal of Geophy. Res.*, 93:7993–8008.

STATISTICS FOR SPATIAL DATA

by: Noel Cressie

1991. John Wiley & Sons. 900 pp. $95 (hardcover); ASPRS Members, $80. Stock # 4629.

Statistics for Spatial Data presents a unified account of the diverse literature and consolidates fragmented statistical methods into a comprehensive, single-source reference. It examines both theoretical and applied aspects of current spatial statistical methods and explores new methods to reveal how spatial statistical models can be used to solve important problems in diverse areas of science and engineering.

The author clearly delineates the three most vigorous areas of growth and offers new models, inferences, and results at the frontiers of the subject. In addition, the author demystifies the "folklore" surrounding spatial statistics and unifies a previously disparate subject under a common approach and a common notation.

Though often theoretical in nature, coverage has been designed to be accessible to all scientists and engineers with solid quantitative skills. The book includes highly detailed treatments of such integral areas as:

- Geostatistical data, including exploratory spatial data analysis, spectral theory, spatial scale, simulation methods, and applications

- Models of spatial lattice data—particularly Markov random fields—their computational aspects and applications
- Asymptotics and finite sample approximations, including discussion of spatial bootstrapping and a view of statistical image analysis
- Spatial point patterns and inference for random set models

Chapters:

- Statistics for Spatial Data
- Geostatistics
- Spatial Prediction and Kriging
- Applications of Geostatistics
- Special Topics in Statistics for Spatial Data
- Spatial Models on Lattices
- Inference for Lattice Models
- Spatial Point Patterns
- Modeling Objects

**For Ordering Information,
See the ASPRS Store.**